HHS Public Access

Author manuscript

Nat Immunol. Author manuscript; available in PMC 2018 April 18.

Published in final edited form as:

Nat Immunol. 2018 January ; 19(1): 29–40. doi:10.1038/s41590-017-0002-1.

Atad3a suppresses Pink1-dependent mitophagy to maintain homeostasis of hematopoietic progenitor cells

Guoxiang Jin[1,2,3], **Chuan Xu**[1,2,3,4], **Xian Zhang**[2,3], **Jie Long**[2,3,5], **Abdol Hossein Rezaeian**[3], **Chunfang Liu**[2,3], **Mark E. Furth**[6], **Steven Kridel**[2], **Boris Pasche**[2], **Xiu-Wu Bian**[1,*], and **Hui-Kuan Lin**[2,3,7,8,*]

[1]Institute of Pathology and Southwest Cancer Center, Southwest Hospital, Third Military Medical University, Chongqing, China

[2]Department of Cancer Biology, Wake Forest School of Medicine, Winston-Salem, NC, USA

[3]Department of Molecular and Cellular Oncology, The University of Texas MD Anderson Cancer Center, Houston, TX, USA

[4]Department of Oncology, Chengdu Military General Hospital, Chengdu, Sichuan, China

[5]Department of Pathology School of Basic Medical Science, Guangzhou Medical University, Guangzhou, Guangdong, China

[6]Wake Forest Innovations, Wake Forest Baptist Medical Center, Winston-Salem, NC, USA

[7]Graduate Institute of Basic Medical Science, China Medical University, Taichung, Taiwan

[8]Department of Biotechnology, Asia University, Taichung, Taiwan

Abstract

Although deletion of certain autophagy-related genes has been associated with defects in hematopoiesis, it remains unclear whether hyperactivated mitophagy affects the maintenance and differentiation of hematopoietic stem cells (HSCs) and committed progenitor cells. Here we report that targeted deletion of the gene encoding the AAA+-ATPase Atad3a hyperactivated mitophagy in mouse hematopoietic cells. Affected mice showed reduced survival, severely decreased bone-marrow cellularity, erythroid anemia and B cell lymphopenia. Those phenotypes were associated with skewed differentiation of stem and progenitor cells and an enlarged HSC pool. Mechanistically, Atad3a interacted with the mitochondrial channel components Tom40 and Tim23

[*]**Correspondence and requests for materials** should be addressed to X.-W.B. or H.-K.L. bianxiuwu@263.net; hulin@wakehealth.edu.

Guoxiang Jin and Chuan Xu contributed equally to this work

Author contributions

G.J., C.X., X.-Z. and J.L. performed the experiments; A.H.R., C.L., S.K. and B.P. provided technical support, critical comments and suggestions; M.E.F. edited the paper; and G.J., X.-W.B. and H.-K.L. designed the experiments, analyzed the data and wrote the paper.

Competing interests

The authors declare no competing financial interests.

Additional information

Supplementary information is available for this paper at https://doi.org/10.1038/s41590-017-0002-1.

and served as a bridging factor to facilitate appropriate transportation and processing of the mitophagy protein Pink1. Loss of Atad3a caused accumulation of Pink1 and activated mitophagy. Notably, deletion of *Pink1* in *Atad3a*-deficient mice significantly 'rescued' the mitophagy defect, which resulted in restoration of the progenitor and HSC pools. Our data indicate that Atad3a suppresses Pink1-dependent mitophagy and thereby serves a key role in hematopoietic homeostasis.

Mitochondria are multifunctional cellular organelles involved in energy metabolism, the production of reactive oxygen species (ROS), apoptosis, signal transduction and nuclear genome transcription[1–3]. Mitochondrial aberrations have been reported in various hematopoietic disorders[4–6].

The role of mitochondria in hematopoiesis is complicated. Mitochondrial contents and activity are maintained at low levels in HSCs to avoid ROS damage[7–9]. However, defective mitochondrial energy metabolism can cause depletion of HSCs, which indicates that mitochondria might be also required for HSCs[10–12]. Notably, mitochondrial contents and activity increase during differentiation and progenitor expansion[7–9]. Thus, the mitochondrial contents might be necessarily maintained at a steady state.

Mitochondrial homeostasis is maintained by both biogenesis and mitophagy. The deletion of genes encoding autophagy-promoting molecules is associated with the accumulation of mitochondria and defective hematopoiesis[13–15], which suggests that mitophagy might be required for hematopoiesis. A specific study of mitophagy has demonstrated that the inhibition of mitophagy by knockdown of the ubiquitin ligase Parkin or Pink1 impairs the self-renewal ability of HSCs[16]. However, since those findings were all derived from autophagy-mitophagy-inhibition models, there is a lack of evidence and mechanistic understanding of the effect of hyperactivated mitophagy on the maintenance of HSCs and the differentiation of those stem cells and committed hematopoietic progenitor cells.

The mitochondrial surface receptors for the ubiquitin-like protein LC3, including Nix, Bnip3 and Func1, can recruit LC3 and trigger mitophagy[17–19]. On the other hand, the Pink1–Parkin pathway activates mitophagy in an ubiquitination-dependent manner. Mitochondrial damage causes Pink1 to accumulate on the mitochondrial surface and recruits Parkin to ubiquitinate multiple mitochondrial proteins. Ubiquitinated proteins recruit LC3 through ubiquitin-binding adaptors to activate mitophagy[20, 21]. In contrast, healthy mitochondria escape from mitophagy by importing Pink1 for processing and degradation and thus restrict the abundance of Pink1 (ref.[22]). Two complexes in the outer membrane and inner membrane, the TOM and TIM complexes, respectively, are required for the import of Pink1 through the membranes[23]. However, the molecular mechanism by which Pink1 is transported from the TOM complex to the TIM complex remains poorly understood.

The AAA+-ATPase (‘ATPase associated with diverse cellular activities’) Atad3a was identified as a mitochondrial protein that spans the inner membrane with its two terminal domains located in the outer membrane and the matrix[24]. Deletion of *Atad3a* in mice causes embryonic death at the early post-implantation stage, during which increased mitochondrial activity is required[25]. However, the underlying mechanism by which Atad3a regulates

mitochondrial homeostasis and activity remains unclear. Interestingly, a published study has shown that Atad3a variant Atad3a^{Arg528Trp} in the fibroblasts of a single patient was associated with activation of mitophagy[26], indicative of a potential role for Atad3a in the regulation of mitophagy.

Here we report the generation of mice with conditional knockout of *Atad3a* in the hematopoietic system. We found that Atad3a bridged between the TOM complex and TIM complex to facilitate the import of Pink1 into mitochondria for processing. Atad3a prevented aberrant accumulation of Pink1 and the consequent recruitment of Parkin to the mitochondria. Atad3 thus functions as a suppressor of mitophagy and has a key role in maintaining mitochondrial homeostasis.

Results

Atad3a deletion skews hematopoietic differentiation

We found that HSCs and committed progenitor cells had higher expression of Atad3a than that of mature hematopoietic cells (Fig. 1a). Thus, we concluded that Atad3a might be specifically required in HSCs and progenitor cells. We therefore generated *Atad3a*$^{fl/fl}$Mx1Cre mice, in which Cre recombinase activity is induced by the synthetic analog of double-stranded RNA poly(I:C) to effect deletion of *Atad3a* specifically in adult hematopoietic cells[11, 27] (Supplementary Fig. 1a,b). Treatment with poly(I:C) did not affect lineage-marker-positive (Lin+) cell populations in Mx1Cre mice (Supplementary Fig. 1c) but caused impaired survival of *Atad3a*$^{fl/fl}$Mx1Cre mice (Fig. 1b), with a significant reduction in total cells in the bone marrow, spleen and thymus (Fig. 1c–e), as well as a progressive decrease in white blood cells, lymphocytes, red blood cells, platelets and hemoglobin in the peripheral blood (Fig. 1f). Consistent with that, deletion of *Atad3a* led to severe anemia and B cell lymphopenia in bone marrow, as indicated by a reduction of Ter119$^+$ erythroid cells and B220$^+$ lymphocytes (Fig. 1g and Supplementary Fig. 1d); however, the proportion of Gr1$^+$Mac1$^+$ myeloid cells was increased (Fig. 1g and Supplementary Fig. 1d). Collectively, these results showed that Atad3a was crucial for normal hematopoiesis.

Atad3a is an intrinsic regulator of hematopoiesis

To determine whether *Atad3a* is an intrinsic regulator of hematopoiesis, we isolated CD45.2+ *Atad3a*$^{fl/fl}$ or *Atad3a*$^{fl/fl}$Mx1Cre bone marrow cells 1 d after treatment of the mice with poly(I:C), then transplanted the cells into lethally irradiated CD45.1+ wild-type recipient mice. Mice that received *Atad3a*-deficient (*Atad3a*$^{fl/fl}$Mx1Cre) bone marrow died rapidly, whereas recipients given transplantation of *Atad3a*$^{fl/fl}$ donor cells all survived (Fig. 2a). Thus, the *Atad3a*-deficient hematopoietic cells had cell-autonomous defects.

We then reconstituted the bone marrow of lethally irradiated CD45.1$^+$ wild-type recipient mice with CD45.2$^+$ *Atad3a*$^{fl/fl}$ or *Atad3a*$^{fl/fl}$Mx1Cre cells without prior activation of Cre. After 6 weeks, the recipient mice received treatment with poly(I:C) to induce Cre activity, and bone marrow cells were assessed 10 d later. Successful reconstitution was demonstrated by CD45.2$^+$ staining of the majority of bone marrow and peripheral cells (Fig. 2b and

Supplementary Fig. 2a,b). The mice reconstituted with *Atad3a*$^{fl/fl}$Mx1Cre bone marrow cells displayed diminished B220+ B cells, depletion of Ter119+ erythroid cells and enhancement of Gr1+Mac1+ myeloid cells (Fig. 2b and Supplementary Fig. 2b), which recapitulated the phenotype of the donor mice. These results confirmed the cell-intrinsic effect of Atad3a on hematopoiesis.

We next performed competitive bone-marrow transplantation by transplanting CD45.2$^+$ *Atad3a*$^{fl/fl}$ or *Atad3a*$^{fl/fl}$Mx1Cre bone-marrow cells (1×10^6), without induction via poly(I:C), together with CD45.1$^+$ wild-type competitor bone-marrow cells (0.5×10^6), into lethally irradiated wild-type recipient mice. The resulting chimeric mice were successfully reconstituted, as shown by a similar frequency of CD45.2$^+$ donor-derived peripheral blood cells at week 5 (Fig. 2c). At 6 weeks after transplantation, the chimeric mice received poly(I:C) to induce Cre activity. The mice reconstituted with *Atad3a*$^{fl/fl}$Mx1Cre bone marrow showed a modest but significant progressive reduction of donor derived CD45.2$^+$ peripheral blood cells; in contrast, the mice reconstituted with *Atad3a*$^{fl/fl}$ CD45.2$^+$ bone marrow showed no decrease in the CD45.2$^+$ population (Fig. 2c). The circulating CD45.2$^+$Mac1$^+$ myeloid-lineage cells were greater in abundance in the *Atad3a*-deficient chimeric mice than in the *Atad3a*$^{fl/fl}$ chimeric mice (Fig. 2d). In contrast, there were fewer donor-derived *Atad3a*-deficient CD45.2$^+$B220$^+$ B cells than *Atad3a*$^{fl/fl}$ CD45.2$^+$B220$^+$ B cells in the peripheral blood (Fig. 2e). As in peripheral blood, we observed a decreased frequency of *Atad3a*-deficient CD45.2$^+$B220$^+$ lymphocytes but an increased frequency of *Atad3a*-deficient CD45.2$^+$Mac1$^+$ myeloid cells in bone marrow of the chimeric recipient mice 12 weeks after treatment with poly(I:C) (Fig. 2f and Supplementary Fig. 2c). Since Ter119$^+$ cells were negative for both CD45.2 and CD45.1, the effect of *Atad3a* deletion on erythropoiesis could not be determined in this competitive bone-marrow-transplantation assay (Supplementary Fig. 2d). Consistent with the reduction in donor-derived *Atad3a*-deficient CD45.2$^+$B220$^+$ cells, the frequency of CD45.2$^+$ cells in the B220$^+$ population was decreased (Supplementary Fig. 2e,g). In contrast, the frequency of CD45.2$^+$ cells in Mac1$^+$ population remained constant (Supplementary Fig. 2f,g). The enhanced frequency of donor-derived *Atad3a*-deficient CD45.2$^+$Mac1$^+$ cells might have been due to compensation for the reduction in the CD45.2$^+$B220$^+$ population. We concluded that Atad3a was required in a cell-intrinsic manner for appropriate hematopoiesis.

Atad3a regulates stem and progenitor cells

To investigate how Atad3a regulates hematopoiesis, we assessed HSCs and progenitor cells in *Atad3a*-deficient bone marrow. We used a gating strategy with the signaling-lymphocytic-activation-molecule receptors CD150 and CD48 to identify HSC populations[28–30] (Supplementary Fig. 3a). Subsequent to Cre-mediated deletion of *Atad3a*, the frequency and number of cells in ‘early’ HSC compartments and progenitor populations consistently increased. These included the following: Lin$^-$Sca-1$^+$cKit$^+$ (LSK) progenitor cells; long-term LSK CD150$^+$CD48$^-$ HSCs (LT-HSCs); short-term LSK CD150$^-$CD48$^-$ HSCs (ST-HSCs); and LSK CD150$^-$CD48$^+$ multipotent progenitors (MPPs) (Fig. 3a–c). The frequency of MPPs, but not that of HSCs, in the LSK compartment was also increased (Supplementary Fig. 3b).

The enlarged populations of LSK cells, HSCs and MPPs might have resulted from increased proliferation, increased cell survival and/or decreased differentiation. Incorporation of the thymidine analog BrdU into *Atad3a*-deficient cells was less than that in *ATAD3A*$^{fl/fl}$ cells (Supplementary Fig. 3c), which suggested impaired proliferation of the former cells. *Atad3a* deficiency also increased cellular apoptosis (Supplementary Fig. 3d). These results indicated that the accumulation of HSCs, MPPs and LSK cells in *Atad3a*-deficient bone marrow might have been caused by blocked commitment to or differentiation into the hematopoietic lineage.

HSCs and LSK cells differentiate into common lymphoid progenitors (CLPs) and common myeloid progenitors (CMPs). CMPs further differentiate into megakaryocyte erythroid progenitors (MEPs) and granulocyte macrophage progenitors (GMPs)[31]. Deletion of *Atad3a* caused a decrease in the absolute number of CMPs, although the frequency of CMPs was not significantly reduced (Fig. 3d–f). The frequency of CMPs in the *Atad3a*-deficient Lin^{-}Sca-1c^{-}Kit^{+} compartment was also lower than the frequency of such cells in the *Atad3a*$^{fl/fl}$ counterpart (Supplementary Fig. 3e). To our surprise, *Atad3a* deficiency increased the CLP population (Fig. 3d,e and Supplementary Fig. 3f). We inferred that Atad3a not only was required for the differentiation but was also critical for the fate ‘decision’ from LSK cell to CMP but not from LSK cell to CLPs.

Furthermore, Atad3a appeared to be necessary for the differentiation and fate ‘decision’ from CMP to MEP but not that from CMP to GMP. Deletion of *Atad3a* severely reduced the MEP population but increased the GMP population (Fig. 3d–f). The result of this disparate effect on the distinct progenitors was manifested by changes in more-mature cells expressing lineage-specific surface markers. We observed an increase in Gr1^{+}Mac1^{+} myeloid cells but a decrease in all stages of Ter119^{+} erythroid cells (Fig. 3g and Supplementary Fig. 3g). Consistent with the reduction in erythroid-progenitor and erythroid-lineage cells, the colony-forming ability of CMPs and MEPs was impaired after deletion of *Atad3a* (Supplementary Fig. 3h).

Despite an increase in CLPs, cells of the B220^{+} lineage decreased after deletion of *Atad3a*, which suggested that *Atad3a* was required for the B cell differentiation at a stage downstream of commitment to lymphoid progenitor cells. In support of that, *Atad3a* deficiency led to a reduction in B220^{+} pro-B cells, pre-B cells and immature IgM^{+} B cells, but the earlier B220^{+} pre-pro-B cell precursors were increased (Fig. 3h and Supplementary Fig. 3i). Thus, Atad3a was required for efficient progression from pre-pro-B cell to pro-B cell.

Our data collectively demonstrated that Atad3a deficiency caused abnormal differentiation defects at multiple hematopoietic progenitor stages.

Atad3a suppresses Pink1-mediated mitophagy

To explore the possibility that the hematopoietic defects that occurred after deletion of *Atad3a* resulted from the deregulation of mitochondrial homeostasis, we assessed the properties of mitochondria in *Atad3a*-deficient bone-marrow cells. *Atad3a* deficiency caused a significant reduction in mitochondrial mass in various bone- marrow populations (Fig. 4a

and Supplementary Fig. 4a). However, the average mitochondrial membrane potential of *Atad3a*-deficient bone-marrow cells, on the basis of mitochondrial content, was not reduced but was instead increased, as assessed by the ratio of cellular membrane potential to mitochondrial mass (Fig. 4b). This might have partially compensated for the loss of mitochondrial mass.

Consistent with the decreased mitochondrial mass, deletion of *Atad3a* diminished both the basal oxygen-consumption rate and the maximal oxidative capacity (Fig. 4c). Although mitochondrial deregulation can alter the cellular ROS level and thus lead to defective maintenance of HSCs[32,33], we found no substantial change in ROS production after deletion of *Atad3a* (Supplementary Fig. 4b). The ATP production of *Atad3a*-deficient cells was similar to that of *Atad3a*$^{fl/fl}$ cells (Supplementary Fig. 4c).

Mitochondrial mass can be regulated by organelle biogenesis, which is affected by a series of transcription factors and co-activators, including PGCα, PGCβ, Errα, Nrf1 and Tfam[34,35]. However, there was no substantial reduction in expression of the genes encoding these molecules after deletion of *Atad3a* (Supplementary Fig. 4d, left). *Atad3a*-deficient cells and *Atad3a*$^{fl/fl}$ cells also had equivalent expression of the mitochondrial proteins Atp5g1, Cox5a, Cycs and Hsp60, which are encoded by the nuclear genes (Supplementary Fig. 4d, right).

Mitochondrial mass can be regulated by mitophagy. Transmission-electron-microscopy analysis revealed that mitophagy occurred in *Atad3a*-deficient LSK cells but not in *Atad3a*$^{fl/fl}$ cells (Fig. 4d), which indicated that the loss of *Atad3a* activated mitophagy to degrade mitochondria.

Mitophagy-dependent mitochondrial degradation can be prevented by the autophagy inhibitors chloroquine or bafilomycin A1. We quantified mitochondrial loss sensitive to chloroquine or bafilomycin A1 to quantify mitophagy relatively. Each drug prevented the loss of mitochondria induced by deletion of *Atad3a* (Fig. 4e and Supplementary Fig. 4e).

We further purified HSCs, MPPs and Lin^{-} progenitor cells and quantified mitochondrial mass by measuring the ratio of mitochondrial DNA to nuclear DNA. This ratio was lower in purified *Atad3a*-deficient cells than in *Atad3a*$^{fl/fl}$ cells, and this reduction was significantly prevented by chloroquine (Fig. 4f). Collectively, our data demonstrated that loss of Atad3a activated mitophagy to degrade mitochondria.

Mitophagy can be induced by stresses to remove damaged mitochondria with lower membrane potential than that of healthy mitochondria[15,36]. Atad3a deficiency not only caused a reduction in the abundance of damaged mitochondria with low potential but also significantly decreased the abundance of healthy mitochondria with high potential (Fig. 5a–c). These data suggested that Atad3a was needed to suppress the mitophagy of healthy mitochondria.

We sought to demonstrate mitophagy flux by measuring co-localization of the mitochondrial marker Tom20 with the lysosomal marker Lamp2a. Knockdown of Atad3a by short hairpin RNA (shRNA) significantly increased the co-colocalization of Tom20 with Lamp2a either in

the absence of leupeptin, a lysosomal proteolysis inhibitor, or in its presence (Fig. 5d,e). We also confirmed mitophagy flux by accumulation of the autophagy marker LC3-II in the intact mitochondrial fraction isolated from *Atad3a*-deficient Lin^- progenitor cells in both the presence of chloroquine and its absence (Fig. 6a and Supplementary Fig. 5a). Consistent with that, autophagy flux (the ratio of LC3-II to LC3-I) was increased after deletion of *Atad3a* (Fig. 6a, bottom).

The accumulation of Pink1 and subsequent recruitment of Parkin to the mitochondrial outer membrane have been shown to trigger mitophagy[20,21,37]. Loss of Atad3a led to increased abundance of Pink1 (Supplementary Fig. 5b) and accumulation of Pink1 and Parkin in the mitochondrial fraction both with and without chloro- quine treatment (Fig. 6a, top). Parkin ubiquitinates multiple mitochondrial proteins. Consistent with that, we observed a profound increase in the polyubiquitination of global mitochondrial proteins after deletion of *Atad3a* (Fig. 6a, top). These data suggested that Atad3a suppressed Pink1-mediated mitophagy. To further test that proposal, we generated HEK293T human embryonic kidney cells in which Atad3a was knocked down or both Atad3a and Pink1 were knocked down. Knockdown of Atad3a increased the abundance of Pink1, diminished mitochondrial mass and led to the accumulation of LC3-II, Pink1 and Parkin and of polyubiquinated proteins in the mitochondrial fraction (Fig. 6b,c). Notably, all of those phenotypes were ‘rescued’ by simultaneous knockdown of Pink1 expression (Fig. 6b,c). We did not detect any change in mitochondrial mass after knockdown of Pink1 alone (Supplementary Fig. 5c).

The cleavage and degradation of Pink1 occurs after its import into the inner mitochondrial membrane[22,38]. That processing depends on both the mitochondrial outer-membrane complex (TOM) and the mitochondrial inner-membrane complex (TIM)[23]. However, it is unclear which cellular factors mediate the transport of Pink1 from the outer membrane to the inner membrane. We found that the endogenous Atad3a interacted with both Tom40 and Tim23, the core components of the TOM complex and TIM complex, respectively (Fig. 6d). Thus, Atad3a might serve as a bridging factor to facilitate the transport of Pink1. We further showed that Pink1 interacted with Atad3a *in vivo* and *in vitro* (Supplementary Fig. 5d,e). That interaction was lost in cells in which Tom40 was knocked down (Fig. 6e). These findings suggested that in normal, healthy cells under physiological conditions, Pink1 might be presented to Atad3a through the TOM complex and then be transported to the TIM complex.

Loss of membrane potential caused by treatment with a combination of oligomycin and antimycin (OA) or with CCCP (a chemical inhibitor of oxidative phosphorylation) inhibits the import of Pink1 and leads to mitophagy[20,38,39]. However, the link between membrane potential and the import of Pink1 has remained elusive. Treatment with OA abolished the interaction between Atad3a and Tim23 but not the interaction of Atad3a with Tom40 (Fig. 6d). That supported the hypothesis that loss of membrane potential induced mitophagy by disrupting an Atad3a–Tim23 complex and thereby blocked the transport of Pink1 (Supplementary Fig. 5f). Consistent with that, treatment with OA severely inhibited the interaction of Pink1 with Tim23 (Fig. 6f). Although treatment with OA or CCCP also decreased the co-immunoprecipitation of Atad3a or Tom40 with Pink1, as determined by

their lower ratio to Pink1 than the ratio without treatment with OA or CCCP (Fig. 6f and Supplementary Fig. 5g), the reduction in these ratios was due to the accumulation of Pink1.

To further investigate whether Atad3a was indeed required for the import of Pink1, we assessed the effects of its depletion on the detection of complexes of Pink1 with Tom40, Tim23 or the matrix Pink1 protease MPPβ, Knockdown of Atad3a largely decreased the interaction of Pink1 with Tim23 or MPPβ (Fig. 6g). We also performed an *in vitro* assay of the import of Pink1 using isolated mitochondria. Mitochondria from cells in which Atad3a was knocked down showed impaired import of Pink1 relative to that of cells mitochondria isolated from control cells in which Atad3a was not knocked down, as determined by the accumulation of full-length Pink1 protein and a relatively decreased abundance of its cleaved form (Fig. 6h).

Atad3a is a mitochondrial AAA+-ATPase whose N terminus interacts with the outer membrane[24]. We next investigated whether the ATPase activity or N terminus of Atad3a was required for the import of Pink1. For this, we generated the mutants Atad3a^{E412Q}, which lacks ATPase activity, and Atad3a^{dN50}, which lacks the 50 amino acids of its N terminus[24]. Similar to wild-type Atad3a, Atad3a^{E412Q} interacted with Tom40, Tim23 and Pink1 (Fig. 6i). In cells in which Atad3a was knocked down, restoration of Atad3a with either wild-type Atad3a or Atad3a^{E412Q} 'rescued' the abnormal accumulation of Pink1, the impaired interaction of Pink1 with Tim23 and the defective *in vitro* import of Pink1 (Fig. 6j,k). In contrast, Atad3a^{dN50} neither interacted with Tom40 and Pink1 nor 'rescued' the *Atad3a*-deficient phenotypes (Fig. 6i–k). We noticed an additional band (an intermediate product) slightly below full-length Pink1 in the *in vitro* importation assay (Fig. 6k, lanes 1, 3, 5). Pink1 is sequentially processed by the proteases MPP and Parl[22]. The intermediate product was probably MPP-processed Pink1 that was not fully cleaved by Parl in the *in vitro* assay. Our data showed that the N terminus of Atad3a but not its ATPase activity was required for its importation.

Collectively, our data indicated a working model in which Atad3a serves as a bridging factor to facilitate the transport of Pink1 from the outer membrane of the mitochondria to its inner membrane for processing and thus maintains a low abundance of Pink1 and prevents mitophagy (Supplementary Fig. 5h).

Atad3a regulates hematopoiesis by suppressing Pink1-dependent mitophagy

To determine whether activation of mitophagy is responsible for the aberrant hematopoietic differentiation in *Atad3a*-deficient bone marrow, we investigated whether the autophagy–mitophagy inhibitor chloroquine could reverse the phenotypic changes induced in the *Atad3a*$^{fl/fl}$Mx1Cre mice. We confirmed by immunoblot analysis that treatment with this drug did not compromise the efficiency of Cre-mediated deletion of *Atad3a* (Fig. 7a) and observed that chloroquine did restore the number of total cells in bone marrow in which *Atad3a* was deleted (Fig. 7b). Moreover, treatment of *Atad3a-deficient* mice with chloroquine significantly 'rescued' both the frequency and number of LT-HSCs, ST-HSCs, MPPs and LSK cells (Fig. 7c–e). Chloroquine also reversed the reduction in CMPs and MEPs and eliminated the elevation in GMPs and CLPs (Fig. 7f–h and Supplementary Fig. 6a).

We then investigated whether Pink1-dependent activation of mitophagy contributed to the defects seen in *Atad3a*-deficient bone marrow by crossing *Atad3a*$^{fl/fl}$Mx1Cre with *Pink1*$^{-/-}$ mice and establishing inducible double-deficient mice. Deletion of *Pink1* in *Atad3a*-deficient mice prolonged their survival, completely restored the mitochondrial mass, abolished the recruitment of LC3-II to mitochondria and repressed the polyubiquitination of mitochondrial proteins (Fig. 8a–c), which suggested that deletion of *Pink1* suppressed the mitophagy activated by *Atad3a* deficiency. Accordingly, the mitochondrial membrane potential and oxygen-consumption defects in *Atad3a*-deficient cells were also significantly 'rescued' by deletion of *Pink1* (Fig. 8d,e). Consequently, loss of *Pink1* restored the total bone-marrow cellularity that was reduced with *Atad3a* deficiency (Fig. 8f). Moreover, deletion of both *Pink1* and *Atad3a* significantly 'rescued' the proportion and absolute number of most of the stem and progenitor cell pools (with the exception of the number of CLPs), including the frequency of LT-HSCs, ST-HSCs, MPPs, LSK cells, GMPs, MEPs and CLPs and the number of LT-HSCs, ST-HSCs, MPPs, LSK cells, CMPs, GMPs and MEPs (Fig. 8g–j and Supplementary Fig. 6b–d). Collectively, our data suggested that Atad3a-mediated suppression of Pink1- dependent mitophagy was critical for the maintaining the homeostasis of HSCs and progenitor cells.

We also assessed the effects of chloroquine and *Pink1-Atad3a* double knockout on the production of more-mature hematopoietic cells. We found that the reduced proportion of Ter119+ erythroid cells in *Atad3a*-deficient bone marrow was restored slightly by treatment with chloroquine and that the number of Ter119+ cells was partially 'rescued' by both chloroquine and double deficiency in *Pink1* and *Atad3a* (Supplementary Fig. 7a–e). The reduced number of B220+ B cells was also partially restored by chloroquine and deletion of *Pink1*, but the increased number of Mac1+ cells was not (Supplementary Fig. 7a–e). Thus, Pink1-dependent suppression of mitophagy by *Atad3a* partially regulated populations of Lin + cells.

Discussion

The regulation of mitochondrial homeostasis during hematopoiesis has remained puzzling. Studies of mice with deletion of genes encoding essential molecules that promote autophagy (for example, *Rb1cc1* (called *'Fip200'* here), *Atg7* or *Atg12)* have shown that inhibition of autophagy is associated with an accumulation of mitochondria and hematopoietic abnormalities[13–15]. Although all deletion of such genes *(Fip200, Atg7* or *Atg12)* results in myeloid expansion, its effects on HSCs and myeloid progenitor cells are different. Deletion of *Atg7* or *Fip200* results in a decrease in HSCs and severe anemia, but Atg12-knockout mice are healthy with no anemia, and their number of HSCs does not change. In addition, *Atg7* deficiency decreases GMPs while promoting mature myeloid proliferation, but deletion of *Atg12* expands both GMP populations and mature myeloid populations. Such contrasting phenotypes of mice deficient in *Atg12, Atg7* or *Fip200* indicate that the inactivation of autophagy in hematopoiesis is more complicated than the deletion of a single gene encoding an autophagy-promoting molecule.

Mitophagy is a specific form of autophagy. The phenotypes of mice in which autophagy is inactivated might result not just from inhibition of mitophagy or accumulation of

mitochondria. Indeed, Tie2+ HSCs in which Parkin or Pink1 is knocked down[16] or LSK cells with low mitochondrial activity[40] show affected self-renewal ability but not myeloid-biased differentiation. Nevertheless, both of those two papers[16,40] also have their limitations. In the first paper, Parkin or Pink1 was silenced to inhibit mitophagy in the isolated $Tie2^{+}$ HSCs cultured *in vitro*, to prove the impaired population expansion of HSCs after inhibition of mitophagy[16]. It lacks genetic evidence to reflect the *in vivo* physiological conditions. Of note, both *Pink1*-knockout mice and Parkin-knockout mice are viable and display no defects in hematopoietic populations[15]. The second paper shows that 'TMRM^{low}' LSK cells (with low mitochondrial activity) display enhanced self-renewal ability[40]. However, the evidence in support of a role for mitophagy in the self-renewal ability HSCs in this paper[40] is not compelling, as it used only the chemical mitochondrial uncoupler FCCP, which might have other, off-target effects, to activate mitophagy[40]. Therefore, it is still unclear whether mitophagy regulates hematopoiesis in genetic mouse models.

Most notably, all of the currently published reports have sought to inhibit autophagy-mitophagy but not to hyperactivate or promote it. It remains unknown whether enhanced activation of mitophagy displays an opposite phenotype by clearing or diminishing the basal mitochondrial content, relative to the inhibition of mitophagy. Our study has provided critical answers to this important question. We have developed the first genetic mouse model, to our knowledge, with hyperactivation of mitophagy by deleting *Atad3a* in the hematopoietic system and have demonstrated that activation of mitophagy by inhibiting the import of Pink1 into mitochondria diminished the basal mitochondrial content, which led to blocked differentiation at certain stages and skewed stem-cell and progenitor pools. Our findings provide new insight into the critical role of mitophagy maintenance in hematopoiesis. An enhancement in mitophagy leads to abnormal hematopoietic phenotypes.

Published studies using a mitophagy-defective model have demonstrated that suppression of mitophagy blocks the maturation of terminal erythrocytes but increases the abundance of immature erythroid cells[41,42], which suggests that basal mitophagy is required for terminal erythrocyte maturation but not for erythroid progenitor differentiation. However, whether enhanced activation of mitophagy affects erythroid progenitor differentiation and erythroid maturation or not is unclear. Our data derived from the hyperactivated-mitophagy mouse model showed that both progenitor erythroid cells and mature erythroid cells were diminished after mitophagy was induced, which suggests that hyperactivation of mitophagy impairs the differentiation of erythroid lineages at the progenitor stage and leads to the depletion of erythroid-lineage cells. Our data, along with the results of previous studies, collectively demonstrate that defects in basal mitophagy and hyperactivation of mitophagy both lead to blocked erythoid differentiation at different stages.

The kinase Pink1 is a key driver of mitophagy. The majority of Pink1 is rapidly degraded after its import into mitochondria and is processed by the mitochondrial peptidases MPP and Parl[22]. Loss of mitochondrial membrane potential prevents the import of Pink1, which causes its accumulation at the mitochondrial surface. This leads to the recruitment of Parkin, the recruitment of mitochondrial proteins and the activation of mitophagy[20,21]. However, how loss of membrane potential blocks the import of Pink1 has remained unclear. Our data

have shown that accumulation of Pink1 after loss of membrane potential required dissociation of the TIM complex from Atad3a.

Our findings suggest that Atad3a serves as a key factor for the import of Pink1 and its processing to suppress unnecessary mitophagy and therefore maintains the normal differentiation of stem cells and progenitor cells. Thus, Pink1-dependent mitophagy should be suppressed to critically maintain mitochondrial homeostasis and normal pools of stem cells and progenitor cells. Our findings suggest that Pink1-dependent hyperactivation of mitophagy might be associated with some hematopoietic disorders and that targeting excessive mitophagy or Pink1 offers a potential therapeutic strategy for such diseases.

Methods

Methods, including statements of data availability and any associated accession codes and references, are available at https://doi.org/10.1038/s41590-017-0002-1.

Methods

Generation of *Atad3a*$^{fl/fl}$ Mx1Cre and *Atad3a*$^{fl/fl}$ Mx1CrePink1$^{-/-}$ mice

The mouse *Atad3a*-targeting ES cell clone (EPD0159_4_A12) generated by the Wellcome Trust Sanger Institute was obtained from the KOMP Repository (www.komp.org)[43]. The ES clone was used to first establish the *Atad3a* heterogeneous knockout-first mice in the MD Anderson Genetically Engineered Mouse Facility. A paired of *loxP* sites was inserted flanking *Atad3a* exon 2 and a LacZ–neomycin cassette flanked with FRT was inserted in intron 1, which terminated *Atad3a* transcription. The knockout-first mice were then bred with Flp recombinase transgenic mice (provided by X. Lin, MD Anderson Cancer Center) to remove the LacZ–neomycin cassette and obtain the *Atad3a*-conditional-knockout mice *Atad3a*$^{fl/fl}$, which contains the *Atad3a* allele with exon 2 flanked by LoxP sites. *Atad3a*$^{fl/fl}$ mice were bred with Mx1Cre to generate *Atad3a*$^{fl/fl}$Mx1Cre mice. *Atad3a*$^{fl/fl}$ Mx1Cre*Pink1*$^{-/-}$ mice were established by crossing *Atad3a*$^{fl/fl}$ Mx1Cre with *Pink1*$^{-/-}$ mice obtained from the Jackson Laboratory. Inbred sex-matched and age-matched (5–8 weeks old) *Atad3a*$^{fl/fl}$, *Atad3a*$^{fl/fl}$Mx1Cre, *Pink1*$^{-/-}$ and *Atad3a*$^{fl/fl}$ Mx1CrePink1$^{-/-}$ mice were used for further experiments. All mouse experiments were performed under protocols approved by the Institutional Animal Use and Care Committees of The Southwest Hospital, Third Military Medical University, MD Anderson Cancer Center and Wake Forest School of Medicine.

Poly(I:C) and chloroquine-bafilomycin treatment

To induce *Atad3a* deletion in *Atad3a*$^{fl/fl}$Mx1Cre or *Atad3a*$^{fl/fl}$ Mx1CrePink1$^{-/-}$ mice for analyses, all of the *Atad3a*$^{fl/fl}$Mx1Cre, *Atad3a*$^{fl/fl}$ Mx1Cre*Pink1*$^{-/-}$ mice and control group mice were give injection of poly(I:C). Poly(I:C) (Invivogen) was dissolved in 0.9% NaCl and administrated intraperitoneally at a dose of 5 mg/kg every other day, four times. Mice were analyzed on the same day between 10 d and 16 d after injection of poly(I:C), unless otherwise indicated. Chloroquine was administrated intraperitoneally daily at 85 mg/kg. Bafilomycin A1 was prepared in DMSO (20 mg/ml) and was diluted in H_2O containing 5% PEG400, 5% Tween80 and was administrated intraperitoneally daily at 2.5 mg/kg.

Flow cytometry

Bone marrow cells were flushed from both mouse femurs and tibias and were suspended in 2% FCS in PBS without calcium and magnesium. Once lysed in RBC lysis buffer (BioLegend) and washed with the suspension buffer, 1×10^6 cells were used for each set of staining with fluorochrome-conjugated surface marker antibodies from BioLegend, eBioscience or BD Bioscience, unless otherwise indicated. For lineage-cell analysis, bone marrow cells were incubated with the following antibodies: anti-B220 (RA3-6B2), CD43 (S11), CD24 (M1/69), CD19 (6D5), IgM (II/41) for B lymphocytes; anti-Ter119 (Ter-119), CD71 (R17217) for erythroid cells; and anti-Gr1 (RB6-8C5), Mac1 (M1/70) for myeloid cells for 30 min on ice before flow cytometry. For stem cells and progenitors, bone marrow cells were first stained with Biotin-conjugated anti-mouse Lineage Panel (BD Bioscience) for 30 min on ice and washed, followed by incubation with fluorochrome-conjugated streptavidin (BioLegend), anti-Scal-1 (D7, Invitrogen), anti-cKit (2B8) and anti-CD150 (TC15-12F12.2), CD48 (HM48.1) and CD41(MWReg30) for HSCs, anti-CD34 (RAM34) and CD16/32 (2.4G2) for CMPs, MEPs and GMPs, and anti-CD127 (A7R34) and Flt3(A2F10.1) for CLPs, respectively, for an additional 30 min, and subjected to flow cytometry. All flow cytometry was performed on a BD FACSCanto II flow cytometer (BD Bioscience). For cell sorting of the bone marrow, cells were stained with a Biotin anti-mouse lineage marker panel, followed by PE/Cy7-labeled streptavidin. The Lin^- cells were sorted on the BD FACSAria II cell sorter (BD Bioscience). We also used the MACS magnetic cell separation system (Miltenyi Biotech) to enrich Lin^- cells. The enriched Lin^- cells were then stained with anti-Scal-1 (D7, Invitrogen), anticKit (2B8) and anti-CD150 (TC15-12F12.2), anti-CD48 (HM48.1) or anti-CD34 (RAM34), CD16/32 (2.4G2) for further sorting of HSCs and progenitor cells.

Bone-marrow transplantation

For the non-competitive bone-marrow transplantation, 1×10^6 total bone marrow cells isolated from CD45.2+ donor *Atad3a*$^{fl/fl}$ or *Atad3a*$^{fl/fl}$Mx1Cre mice (at day 1 after injection of poly(I:C)) were transplanted into lethally irradiated $CD45.1^+$ recipient mice. The mouse survival after transplantation was monitored. In another experiment, we followed the same procedure with donor cells not exposed to poly(I:C). 6 weeks later, all recipient mice received injection of poly(I:C), and *Atad3a* deletion was induced in *Atad3a*$^{fl/fl}$ Mx1Cre donor cells by poly(I:C). After a further 10 d, the bone marrow cells were analyzed by flow cytometry.

For competitive bone marrow transplantation, 1×10^6 $CD45.2^+$ donor *Atad3a*$^{fl/fl}$ or *Atad3a*$^{fl/fl}$Mx1Cre donor bone marrow cells without poly(I:C) treatment were combined with 0.5×10^6 $CD45.1^+$ competitor cells and were transplanted into lethally irradiated recipient mice. 6 weeks later, all the recipient mice received injection of poly(I:C), and *Atad3a* deletion was induced in *Atad3a*$^{fl/fl}$Mx1Cre donor cells by poly(I:C). 12 weeks later, the donor-derived bone-marrow cells were harvested and analyzed by flow cytometry.

Measurement of mitochondrial mass, membrane potential and cell ROS production

Bone marrow cells were isolated and stained for cell-surface markers, followed by incubation with 50 nM MitoTracker Green FM (or 100 nM MitoTracker Deep Red FM), 100

nM MitoTracker CMXROS, 100 nM TMRM or 5 μM DCFDA (Invitrogen) at 37 °C for 15-20 min and were analyzed by flow cytometry.

Measurement of oxygen consumption and cellular ATP concentration

LSK cells were sorted and seeded in microplate wells with the adhesive reagent Corning Cell-Tak. The oxygen-consumption rate measurement was performed on the Seahorse XF24 analyzer according to the manufacturer's protocol. The Lin^- cells were sorted from isolated control and *Atad3a*-deficient bone marrow cells. The same number of cells was lysed to measure the ATP concentration following the manufacturers protocol of the ATP Determination Kit (Molecular Probes).

Cell apoptosis and proliferation analysis

To determine cell apoptosis, 1×10^6 Lin^- cells were sorted from control and *Atad3a*-deficient bone marrow cells. The cells were fixed, and the frequency of apoptotic cells was measured following the manufacturers protocol for the APO-BrdU TUNEL Assay Kit (Molecular Probes). To determine cell proliferation, the sorted cells were cultured *in vitro* for 48 h and then were incubated with 10 mM BrdU for 1 h in complete medium at 37 °C. The cells were then trypsinized, washed with PBS and stained with FITC-conjugated antibody to BrdU following the manufacturer's protocol for the *In situ* Cell Proliferation Kit (Roche). The frequency of $BrdU^+$ cells, interpreted as actively proliferating cells in S phase, was determined by flow cytometry.

Transmission-electron-microscopy imaging

Lin^- cells were sorted from isolated control and *Atad3a*-deficient bone marrow and subjected to transmission-electron-microscopy imaging in the MD Anderson High Resolution Electron Microscope Facility. In brief, the cells were fixed in 0.1 M cacodylate fixation buffer (3% glutaraldehyde and 2% paraformaldehyde, pH 7.3), washed with 0.1 M sodium cacodylate, and then processed to treatment in 0.1% tannic acid and post-fixation in 1% osmium tetroxide for 30 min, followed by staining in 1% uranyl acetate. After dehydration, the samples were embedded with LX-112 medium which was allowed to polymerize for 2 d in a 60 °C oven before section preparation on an Ultracut microtome (Leica). The sections were then stained with uranyl acetate and lead citrate. The images were taken through the AMT imaging system (Advanced Microscopy Techniques Corp) on a JEM1010 transmission electron microscope (JEOL).

Knockdown of Atad3a, Pink1 and Tom40

shRNA targeting Atad3a, Pink1 or Tom40, ordered from Sigma, was used to establish the HEK293T cells in which those molecules were knocked down. The shRNA we used in this paper included the following:

shAtad3a#1(TRCN0000136391):
CCGGCCTGCACATTTAGGATATGCTCTCGAGAGCATATCCTAAATGTGCAGG
TTTTTTG

shAtad3a#2(TRCN0000231876):
CCGGGCCAGGCAGGTGATGTCTTTGCTCGAGCAAAGACATCACCTGCCTG
GCTTTTTG

shPink1(TRCN0000007101):
CCGGCGGCTGGAGGAGTATCTGATACTCGAGTATCAGATACTCCTCCAGCC
GTTTTTG

shTom40#1(TRCN0000219098):
GTACCGGCAAAGGGTTGAGTAACCATTTCTCGAGAAATGGTTACTCAACCC
TTTGTTTTTTG

shTom40#2(TRCN0000231152):

CCGGCATGTCTCTAGCTGGGAAATACTCGAGTATTTCCCAGCTAGAGACATG
TTTTTG

RT-PCR analysis

Cells were sorted from control and *Atad3a*-deficient mouse bone marrow at day 12 after injection of poly(I:C), and total RNA was isolated using the RNeasy Mini Kit (Qiagen). The mRNA was converted into cDNA following the manufacturer's protocol of the SuperScript III reverse transcriptase kit (Life Technologies) and subjected to RT-PCR.

Immunoblot, immunoprecipitation and immunofluorescence analysis

The cells or mitochondria isolated using a Mitochondria Isolation Kit (Life Technologies) were lysed in RIPA buffer containing protein inhibitor cocktail (Roche) and 10 mM deubiquitinase inhibitor N-ethylmaleimide (NEM), and subjected to immunoblot analysis with antibodies specific for LC3B (3868, Cell Signaling), Pink1 (ab75487, Abcam), Parkin (ab15954, Abcam), ubiquitin (sc-8017, Santa Cruz), Hsp60 (12165, Cell Signaling), Tom40 (sc365467, Santa Cruz), Tim23 (sc-514463), MPPß (16064-1-AP), Flag (F1804, Sigma) and Atad3a (Novus, H00055210). We also used antibodies to Atad3a provided by J. Baudier (Université d'Aix-Marseille) and D. Rousseau from (University Grenoble Alpes)[44]. For immunoprecipitation, cell lysates were prepared from HEK293T cells and were incubated with antibodies to Pink1, Atad3a (H00055210, Novus) and Flag overnight, followed by incubation with 40 µl Protein A/G agarose beads for 2 h. The beads were then washed four times with lysis buffer and subjected to immunoblot analysis. For immunofluorescence staining, HEK293T cells in which Atad3a was knocked down or not were seeded in the culture chamber and were treated with or without 10 µM leupeptin for 3 h, then fixed with 4% PFA, permeabilized with 0.1% Triton and stained with anti-Tom20 (sc-17764, Santa Cruz) and anti-Lamp2a (ab18528, Abcam). Confocal images were taken, and the frequency of co-localization of Tom20 to Lamp2a was quantified with the Jacop plugin of ImageJ.

In vitro mitochondrial importation assay of Pink1

A C-terminal Flag-tagged Pink1 construct (provided by T.L. Schwarz, Boston Children's Hospital)[45] was transfected into HEK293T cells and Pink1 protein was purified. The same amount of Flag-tagged Pink1 was mixed with mitochondria isolated from HEK293T cells in which Atad3a was knocked down or not or from HEK293T cells in which Atad3a was

knocked down and that were engineered to overexpress wild-type or mutant Atad3a, in importation assay buffer containing 20 mM HEPES (pH 7.4), 250 mM Sucrose, 80 mM KAc, 5 mM Mg(Ac)2, 2 mM ATP and 2 mM NADH, followed by incubation at 30 °C for 1 h. The mitochondria were then washed twice and analyzed by immunoblot.

In vitro binding assay

Purified Flag-tagged Pink1 and Myc-tagged Atad3a were incubated in buffer containing 20 mM HEPES (pH7.4), 150 mM NaCl, 5 mM $MgCl_2$, 1 mM DTT, 0.5 mM EDTA, 0.05% NP40 abd 10% glycerol with a proteinase inhibitor cocktail and were rotated at 4 °C overnight, then immunoprecipitated by anti-Myc and analyzed for Pink1 and Atad3a.

Statistical analysis

Kaplan-Meier mouse-survival data were statistically analyzed by the log-rank (Mantel Cox) test. To compare two groups, data were analyzed by a two-sided Student's *t*-test. For more than two groups, the data were analyzed by one-way ANOVA followed by Bonferroni post-hoc test. Data are presented as mean ±s.d. (SD). $P<0.05$ was considered statistically significant. * indicates $P < 0.05$; ** indicates $P < 0.01$; *** indicates $P < 0.001$.

Life Sciences Reporting Summary

Further information on experimental design and reagents is available in the Life Sciences Reporting Summary.

Data availability

The data that support the findings of this study are available from the corresponding author upon request.

Supplementary Material

Refer to Web version on PubMed Central for supplementary material.

Acknowledgments

We thank X. Lin (MD Anderson Cancer Center) for the for FLP transgenic mouse; T.L. Schwarz (Boston Children's Hospital) for the Pink1-encoding plasmid; J. Baudier (Université d[1]Aix-Marseille) and D. Rousseau (University Grenoble Alpes) for antibodies to Atad3a; J. Parker-Thornburg and J. Alana for blastocyst microinjection; D.P. Pollock for microarray analysis; K. Dunner for transmission-electron-microscopy imaging; B. Zhen and S. Zhang for technical assistance; the flow cytometry core facility at MD Anderson Cancer Center and Wake Forest School of Medicine for flow cytometry analysis; D.D. Sarbassov and the members of the Lin laboratory for comments and suggestions; and X. Zhou for the assistance in statistical analysis. Supported by the National Key Research and Development Program of China (2016YFA0101200 to X.-WB.), the National Natural Science Foundation of China (61327902-04 to X.-W.B.), the US National Institutes of Health (R01 CA182424 and R01 CA193813 to H.-K.L.) and Wake Forest University School of Medicine (start-up funds to H.-K.L.).

References

1. Wallace DC, Fan W. Energetics, epigenetics, mitochondrial genetics. Mitochondrion. 2010; 10:12–31. [PubMed: 19796712]
2. Sun MG, et al. Correlated three-dimensional light and electron microscopy reveals transformation of mitochondria during apoptosis. Nat Cell Biol. 2007; 9:1057–1065. [PubMed: 17721514]

3. Salminen A, Kaarniranta K, Hiltunen M, Kauppinen A. Krebs cycle dysfunction shapes epigenetic landscape of chromatin: novel insights into mitochondrial regulation of aging process. Cell Signal. 2014; 26:1598–1603. [PubMed: 24704120]
4. Kim HR, et al. Mitochondrial DNA aberrations of bone marrow cells from patients with aplastic anemia. J Korean Med Sci. 2008; 23:1062–1067. [PubMed: 19119453]
5. Kim HR, et al. Mitochondrial DNA aberrations and pathophysiological implications in hematopoietic diseases, chronic inflammatory diseases, and cancers. Ann Lab Med. 2015; 35:1–14. [PubMed: 25553274]
6. Yao YG, et al. Mitochondrial DNA sequence variation in single cells from leukemia patients. Blood. 2007; 109:756–762. [PubMed: 16946307]
7. Joshi A, Kundu M. Mitophagy in hematopoietic stem cells: the case for exploration. Autophagy. 2013; 9:1737–1749. [PubMed: 24135495]
8. Mantel C, Messina-Graham S, Broxmeyer HE. Upregulation of nascent mitochondrial biogenesis in mouse hematopoietic stem cells parallels upregulation of CD34 and loss of pluripotency: a potential strategy for reducing oxidative risk in stem cells. Cell Cycle. 2010; 9:2008–2017. [PubMed: 20495374]
9. Guan JL, et al. Autophagy in stem cells. Autophagy. 2013; 9:830–849. [PubMed: 23486312]
10. Gan B, et al. Lkb1 regulates quiescence and metabolic homeostasis of haematopoietic stem cells. Nature. 2010; 468:701–704. [PubMed: 21124456]
11. Nakada D, Saunders TL, Morrison SJ. Lkb1 regulates cell cycle and energy metabolism in haematopoietic stem cells. Nature. 2010; 468:653–658. [PubMed: 21124450]
12. Gurumurthy S, et al. The Lkb1 metabolic sensor maintains haematopoietic stem cell survival. Nature. 2010; 468:659–663. [PubMed: 21124451]
13. Liu F, et al. FIP200 is required for the cell-autonomous maintenance of fetal hematopoietic stem cells. Blood. 2010; 116:4806–4814. [PubMed: 20716775]
14. Mortensen M, et al. The autophagy protein Atg7 is essential for hematopoietic stem cell maintenance. J Exp Med. 2011; 208:455–467. [PubMed: 21339326]
15. Ho TT, et al. Autophagy maintains the metabolism and function of young and old stem cells. Nature. 2017; 543:205–210. [PubMed: 28241143]
16. Ito K, et al. Self-renewal of a purified $Tie2^{+}$ hematopoietic stem cell population relies on mitochondrial clearance. Science. 2016; 354:1156–1160. [PubMed: 27738012]
17. Wei H, Liu L, Chen Q. Selective removal of mitochondria via mitophagy: distinct pathways for different mitochondrial stresses. Biochim Biophys Acta. 2015; 1853:2784–2790. [PubMed: 25840011]
18. Novak I, et al. Nix is a selective autophagy receptor for mitochondrial clearance. EMBO Rep. 2010; 11:45–51. [PubMed: 20010802]
19. Liu L, et al. Mitochondrial outer-membrane protein FUNDC1 mediates hypoxia-induced mitophagy in mammalian cells. Nat Cell Biol. 2012; 14:177–185. [PubMed: 22267086]
20. Narendra DP, et al. PINK1 is selectively stabilized on impaired mitochondria to activate Parkin. PLoS Biol. 2010; 8:e1000298. [PubMed: 20126261]
21. Matsuda N, et al. PINK1 stabilized by mitochondrial depolarization recruits Parkin to damaged mitochondria and activates latent Parkin for mitophagy. J Cell Biol. 2010; 189:211–221. [PubMed: 20404107]
22. Greene AW, et al. Mitochondrial processing peptidase regulates PINK1 processing, import and Parkin recruitment. EMBO Rep. 2012; 13:378–385. [PubMed: 22354088]
23. Pickrell AM, Youle RJ. The roles of PINK1, parkin, and mitochondrial fidelity in Parkinson's disease. Neuron. 2015; 85:257–273. [PubMed: 25611507]
24. Gilquin B, et al. The AAA + ATPase ATAD3A controls mitochondrial dynamics at the interface of the inner and outer membranes. Mol Cell Biol. 2010; 30:1984–1996. [PubMed: 20154147]
25. Goller T, Seibold UK, Kremmer E, Voos W. & Kolanus, W Atad3 function is essential for early post-implantation development in the mouse. PLoS One. 2013; 8:e54799. [PubMed: 23372768]

26. Harel T, et al. Recurrent de novo and biallelic variation of ATAD3A, encoding a mitochondrial membrane protein, results in distinct neurological syndromes. Am J Hum Genet. 2016; 99:831–845. [PubMed: 27640307]
27. Kühn R, Schwenk F, Aguet M, Rajewsky K. Inducible gene targeting in mice. Science. 1995; 269:1427–1429. [PubMed: 7660125]
28. Kiel MJ, et al. SLAM family receptors distinguish hematopoietic stem and progenitor cells and reveal endothelial niches for stem cells. Cell. 2005; 121:1109–1121. [PubMed: 15989959]
29. Oguro H, Ding L, Morrison SJ. SLAM family markers resolve functionally distinct subpopulations of hematopoietic stem cells and multipotent progenitors. Cell Stem Cell. 2013; 13:102–116. [PubMed: 23827712]
30. Foudi A, et al. Analysis of histone 2B-GFP retention reveals slowly cycling hematopoietic stem cells. Nat Biotechnol. 2009; 27:84–90. [PubMed: 19060879]
31. Challen GA, Boles N, Lin KK, Goodell MA. Mouse hematopoietic stem cell identification and analysis. Cytometry A. 2009; 75:14–24. [PubMed: 19023891]
32. Miyamoto K, et al. Foxo3a is essential for maintenance of the hematopoietic stem cell pool. Cell Stem Cell. 2007; 1:101–112. [PubMed: 18371339]
33. Tothova Z, et al. FoxOs are critical mediators of hematopoietic stem cell resistance to physiologic oxidative stress. Cell. 2007; 128:325–339. [PubMed: 17254970]
34. Lelliott CJ, Vidal-Puig A. PGC-1beta: a co-activator that sets the tone for both basal and stress-stimulated mitochondrial activity. Adv Exp Med Biol. 2009; 646:133–139. [PubMed: 19536672]
35. Austin S, St-Pierre J. PGC1a and mitochondrial metabolism-emerging concepts and relevance in ageing and neurodegenerative disorders. J Cell Sci. 2012; 125:4963–4971. [PubMed: 23277535]
36. Tal MC, et al. Absence of autophagy results in reactive oxygen species-dependent amplification of RLR signaling. Proc Natl Acad Sci USA. 2009; 106:2770–2775. [PubMed: 19196953]
37. Narendra D, Tanaka A, Suen DF, Youle RJ. Parkin is recruited selectively to impaired mitochondria and promotes their autophagy. J Cell Biol. 2008; 183:795–803. [PubMed: 19029340]
38. Jin SM, et al. Mitochondrial membrane potential regulates PINK1 import and proteolytic destabilization by PARL. J Cell Biol. 2010; 191:933–942. [PubMed: 21115803]
39. Lazarou M, et al. The ubiquitin kinase PINK1 recruits autophagy receptors to induce mitophagy. Nature. 2015; 524:309–314. [PubMed: 26266977]
40. Vannini N, et al. Specification of haematopoietic stem cell fate via modulation of mitochondrial activity. Nat Commun. 2016; 7:13125. [PubMed: 27731316]
41. Mortensen M, et al. Loss of autophagy in erythroid cells leads to defective removal of mitochondria and severe anemia in vivo. Proc Natl Acad Sci USA. 2010; 107:832–837. [PubMed: 20080761]
42. Sandoval H, et al. Essential role for Nix in autophagic maturation of erythroid cells. Nature. 2008; 454:232–235. [PubMed: 18454133]
43. Skarnes WC, et al. A conditional knockout resource for the genome-wide study of mouse gene function. Nature. 2011; 474:337–342. [PubMed: 21677750]
44. Hubstenberger A, Labourdette G, Baudier J, Rousseau D. ATAD 3A and ATAD 3B are distal 1p-located genes differentially expressed in human glioma cell lines and present in vitro anti-oncogenic and chemoresistant properties. Exp Cell Res. 2008; 314:2870–2883. [PubMed: 18639545]
45. Wang X, et al. PINK1 and Parkin target Miro for phosphorylation and degradation to arrest mitochondrial motility. Cell. 2011; 147:893–906. [PubMed: 22078885]

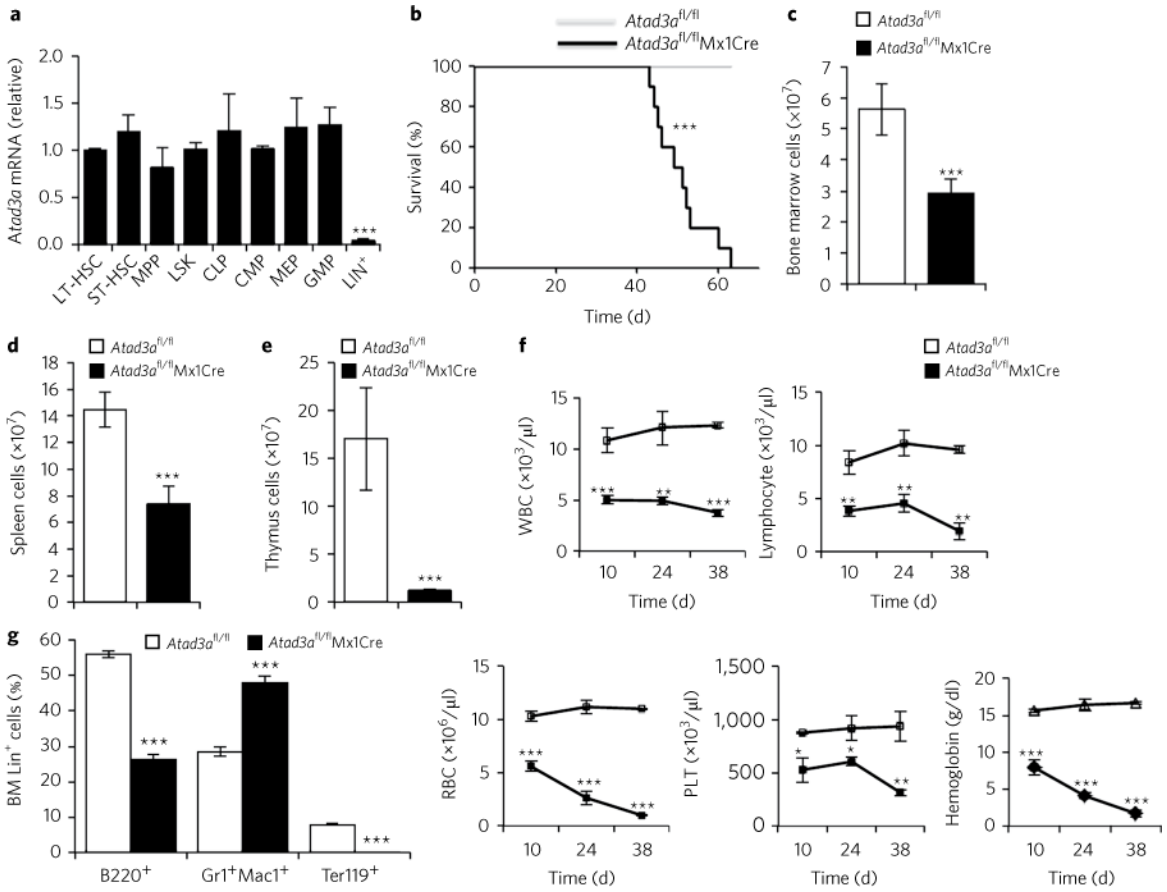

Fig. 1. Deletion of *Atad3a* skews hematopoietic differentiation

a, Expression of *Atad3a* mRNA in various hematopoietic populations (horizontal axis); results are presented relative to those of LT-HSCs. **b**, Survival of *Atad3a*$^{fl/fl}$ and *Atad3a*$^{fl/fl}$Mx1Cre mice (key) after injection of poly(I:C) (Kaplan-Meier analysis). **c–e**, Total cells in the bone marrow (**c**), spleen (**d**) and thymus (**e**) of *Atad3a*$^{fl/fl}$ and *Atad3a*$^{fl/fl}$Mx1Cre mice (key). **f**, Quantification of white blood cells (WBC), lymphocytes, red blood cells (RBC), platelets (PLT) and hemoglobin in the peripheral blood of *Atad3a*$^{fl/fl}$ and *Atad3a*$^{fl/fl}$Mx1Cre mice (key). **g**, Frequency of various cells (horizontal axis) of the bone-marrow (BM) lineage in *Atad3a*$^{fl/fl}$ and *Atad3a*$^{fl/fl}$Mx1Cre mice (key). **P*< 0.05, ***P*<0.01 and ****P*<0.001, LT-HSC versus Lin$^+$ in **a** (one-way analysis of variance (ANOVA) followed by Bonferroni post-hoc test (**a**), log-rank (Mantel Cox) test (**b**) or Student's *t*-test (**c–g**)). Data are representative of two independent experiments (**a**; mean ± s.d. of $n = 3$ biological replicates) or three independent experiments with $n = 10$ mice per group (**b**) or are from two independent experiments (**c–e**,**g** (average); mean± s.d. of $n = 8$ mice per genotype (**c–e**), or $n = 6$ mice per genotype (**g**) or $n \geq 3$ mice per genotype (**f**)).

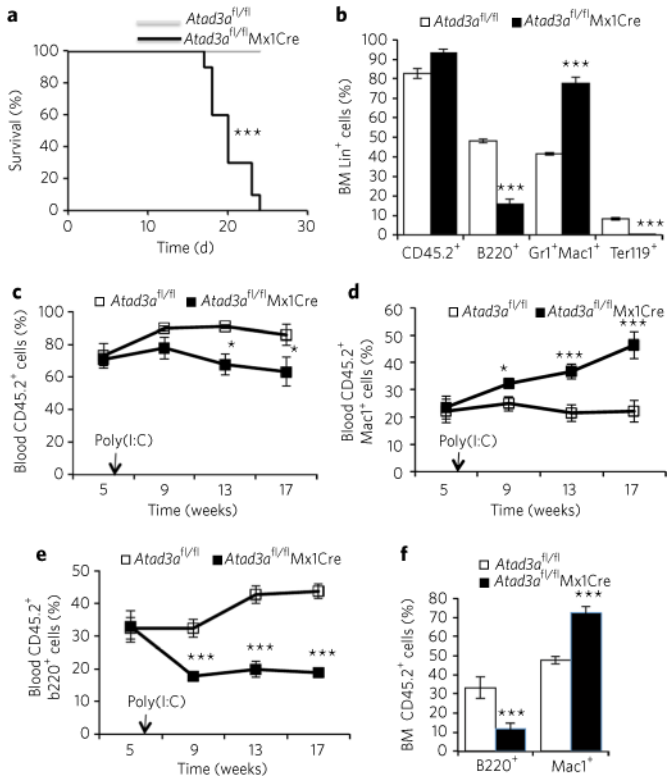

Fig. 2. Atad3a is an intrinsic regulator of hematopoiesis

a, Survival (Kaplan-Meier analysis) of mice given transplantation of *Atad3a*$^{fl/fl}$ *or* *Atad3a*$^{fl/fl}$Mx1Cre bone marrow (key). **b**, Frequency of donor-derived CD45.2$^+$ cells (far left) and various cells (horizontal axis) of the bone-marrow lineage in mice given non-competitive transplantation of *Atad3a*$^{fl/fl}$ or *Atad3a*$^{fl/fl}$Mx1Cre bone marrow (key), assessed by flow cytometry on day 10 after injection of poly(I:C) into the recipient mice. **c–e**, Frequency of donor-derived CD45.2$^+$ cells (**c**), CD45.2$^+$Mac1$^+$ myeloid cells (**d**) or CD45.2$^+$B220$^+$ B cells (**e**) in the peripheral blood of mice given competitive transplantation of *Atad3a*$^{fl/fl}$ or *Atad3a*$^{fl/fl}$Mx1Cre bone marrow (key), assessed by flow cytometry at various times (horizontal axis) after injection of poly(I:C) into the recipient mice (downward arrow). **f**, Frequency of various donor-derived cells (horizontal axis) in the bone marrow of mice given competitive transplantation of *Atad3a*$^{fl/fl}$ or *Atad3a*$^{fl/fl}$Mx1Cre bone marrow (key), assessed 12 weeks after injection of poly(I:C) into the recipient mice. *P< 0.05 and ***P<0.001 (logrank (Mantel Cox) test (**a**) or Student's t-test (**b–f**)). Data are from one experiment representative of two independent experiments (with n = 10 mice per group (**a**); mean ± s.d. of n>4 mice per group (**b–f**)).

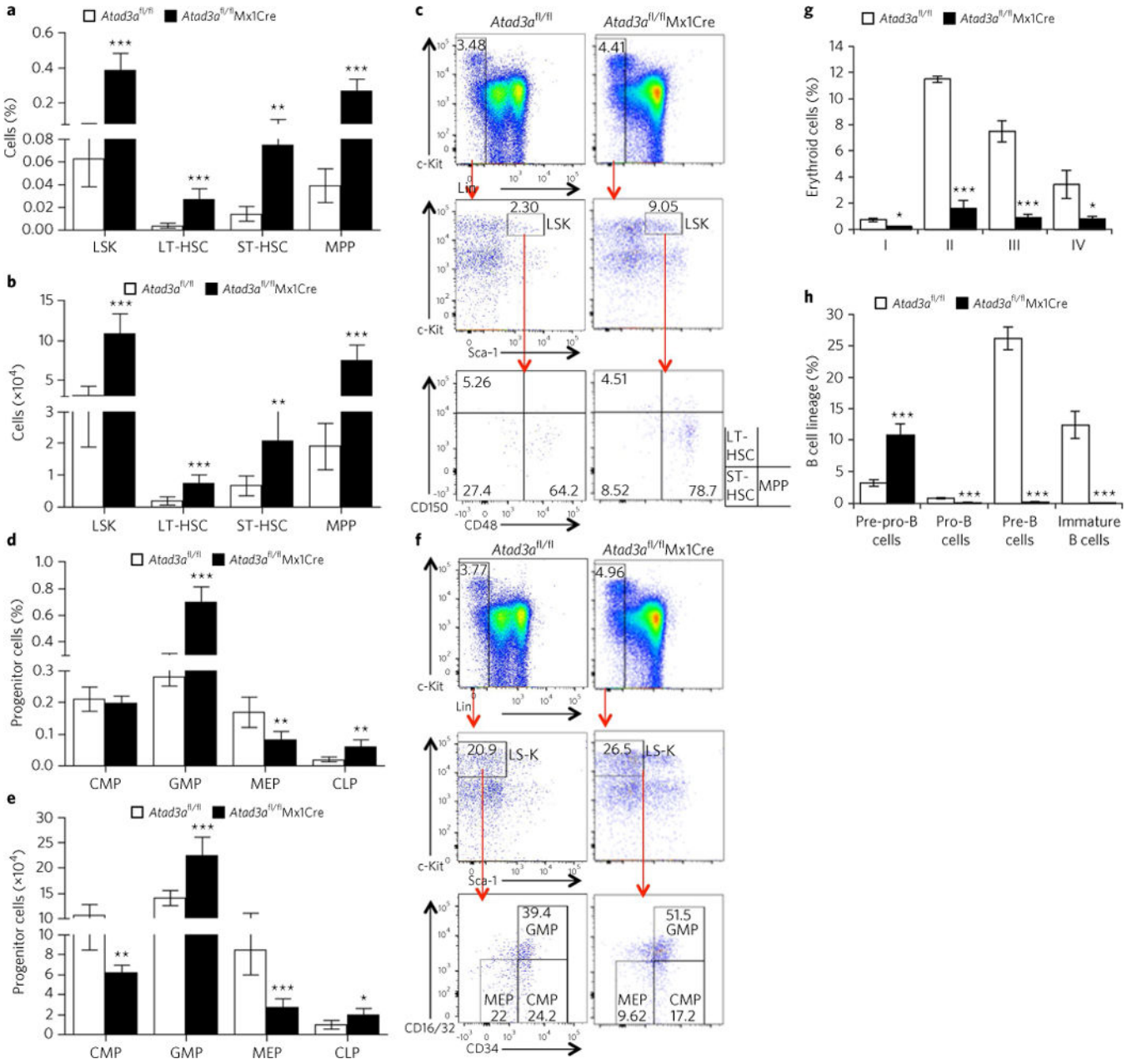

Fig. 3. Loss of *Atad3a* causes defective hematopoiesis at multiple stages

a,**b**, Frequency (**a**) and number (**b**) of LSK cells, LT-HSCs, ST-HSCs and MPPs (horizontal axis) in *Atad3a*$^{fl/fl}$ or *Atad3a*$^{fl/fl}$Mx1Cre bone marrow (key). **c**, Flow cytometry of LSK cells, LT-HSCs, ST-HSCs and MPPs in *Atad3a*$^{fl/fl}$ and *Atad3a*$^{fl/fl}$Mx1Cre bone marrow (above plots). Numbers in or adjacent to outlined areas indicate percent cells in each gate (key, bottom right). **d,e**, Frequency (**d**) and number (**e**) of CMPs, MEPs, GMPs and CLPs (horizontal axis) in *Atad3a*$^{fl/fl}$ or *Atad3a*$^{fl/fl}$Mx1Cre bone marrow (key). **f**, Flow cytometry of CMPs, MEPs and GMPs in *Atad3a*$^{fl/fl}$ or *Atad3a*$^{fl/fl}$Mx1Cre bone marrow (above plots). Numbers in or adjacent to outlined areas indicate percent cells in each gate (LS^{-}K: Lin^{-}Sca-1^{-}cKit^{+}). **g**, Frequency of erythroid cells at various stages, including Ter119^{med}CD71^{hi}

proerythroblasts (I), Ter119^{hi}CD71^{hi} basophilic erythroblasts (II), Ter119^{hi}CD71^{med} late erythroblasts (III) and Ter119^{hi}CD71^{lo} late erythroblasts (IV) (horizontal axis), in *Atad3a*$^{fl/fl}$ or *Atad3a*$^{fl/fl}$Mx1Cre mice (key). **h**, Frequency of B lymphocytes at various stages, including B220^{+}CD19^{-}CD24^{-}CD43^{+}IgM^{-} pre-pro-B cells, B220^{+}CD19^{+}CD24^{+}CD43^{+}IgM^{-} pro-B cells, B220^{+}CD19^{+}CD24^{+}CD43^{-}IgM^{-} pre-B cells and B220^{+}CD19^{+}CD24^{+}CD43^{-}IgM^{+} immature B cells (horizontal axis), in *Atad3a*$^{fl/fl}$ or *Atad3a*$^{fl/fl}$Mx1Cre mice (key). **P*<0.05, ***P*< 0.01 and ****P*<0.001 (Student's *t*-test). Data are from two independent experiments (averaged; mean±s.d. of $n = 8$ mice per genotype (**a,b,h**), $n = 6$ mice per genotype (**d,e**) or $n = 3$ mice per genotype (**g**)).

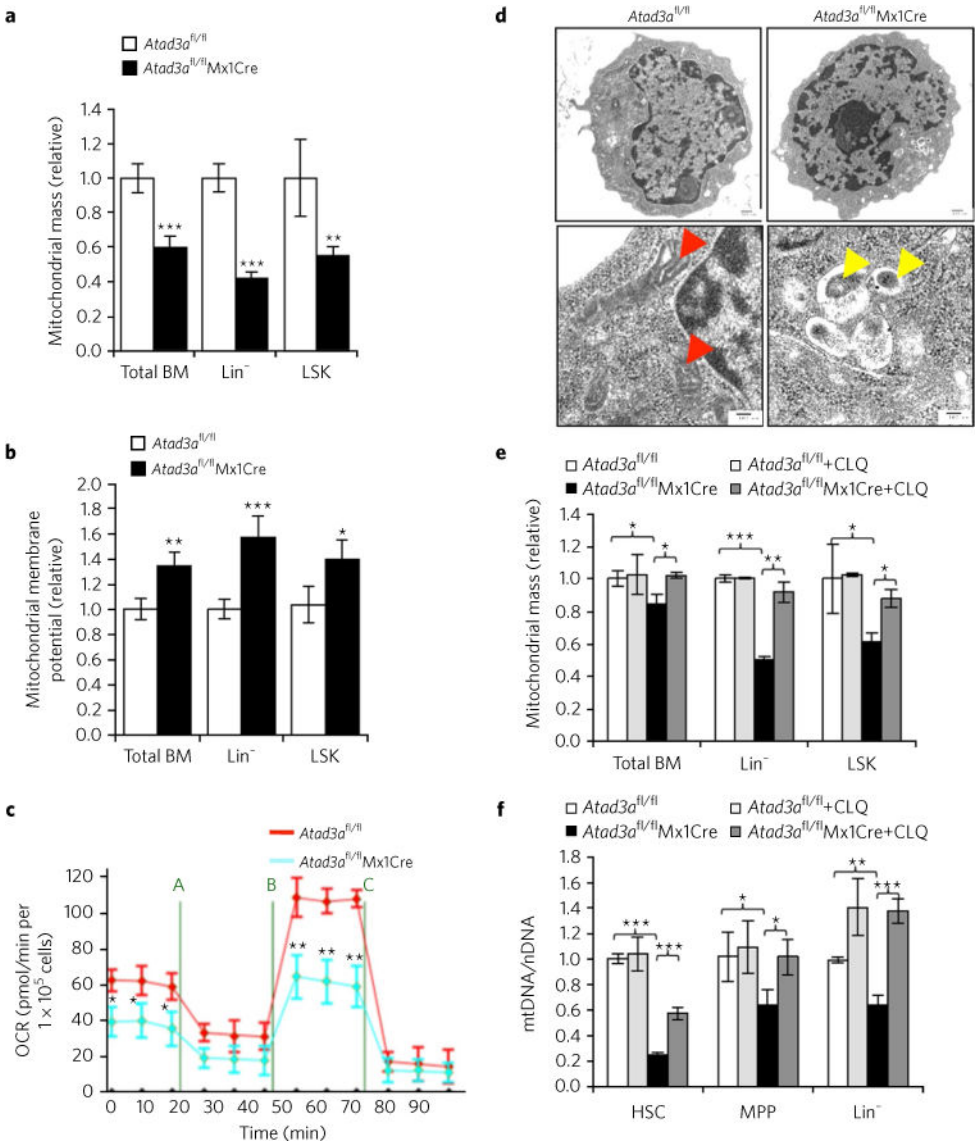

Fig. 4. Loss of *Atad3a* diminishes mitochondrial content and enhances mitophagy

a,**b**, Mitochondrial mass (**a**) and membrane potential (**b**) of various hematopoietic cell populations (horizontal axis) from *Atad3a*$^{fl/fl}$ or *Atad3a*$^{fl/fl}$Mx1Cre mice (key); mass assessed with the green fluorescent mitochondrial stain MitoTracker Green FM (**a**), and membrane potential (assessed with TMRM, a red-orange fluorescent dye sequestered by active mitochondria), calculated as a ratio to mitochondria mass (TMRM/MitoTracker Green FM) (**b**), with both presented relative to results obtained for *Atad3a*$^{fl/fl}$ mice. **c**, Oxygen-consumption rate (OCR) of LSK cells obtained from *Atad3a*$^{fl/fl}$ or *Atad3a*$^{fl/fl}$Mx1Cre mice (key) and then treated sequentially (vertical lines) with 1 μM oligomycin (A), 0.5 μM FCCP (B) and 0.5 μM rotenone and antimycin (C); results presented per 1 × 10^5 sorted LSK cells. **d**, Transmission electron microscopy of LSK cells from *Atad3a*$^{fl/fl}$ or *Atad3a*$^{fl/fl}$Mx1Cre mice (above images); arrows indicate normal mitochondria (red) and mitophagy (yellow). Scale bars, 500 nm (top row) or 100 nm (bottom row). **e**, Mitochondrial mass of *Atad3a*$^{fl/fl}$ or *Atad3a*$^{fl/fl}$Mx1Cre (key) hematopoietic cell populations (horizontal axis) in the presence

(+ CLQ) or absence of chloroquine (key), presented as in **a**. **f**, Ratio of mitochondrial DNA (*Nd4*) to nuclear DNA (*B2m*) (mtDNA/nDNA) in purified *Atad3a*$^{fl/fl}$ or *Atad3a*$^{fl/fl}$Mx1Cre (key) hematopoietic cell populations (horizontal axis) in the presence or absence of chloroquine (key), presented relative to results obtained for *Atad3a*$^{fl/fl}$ mice. **P*<0.05, ** *P*<0.01 and *** *P*<0.001 (Student's *t*-test (**a**–**c**) or one-way ANOVA followed by Bonferroni post-hoc test (**e**,**f**)). Data are from one experiment representative of three independent experiments (**a**,**b**; mean ± s.d. of $n \geq 4$ mice per genotype) or one experiment representative of two independent experiments (**c**–**f**; mean ± s.d. of $n = 3$ mice per genotype (**c**), $n = 4$ mice per group (**e**) or $n = 3$ mice per group (**f**)).

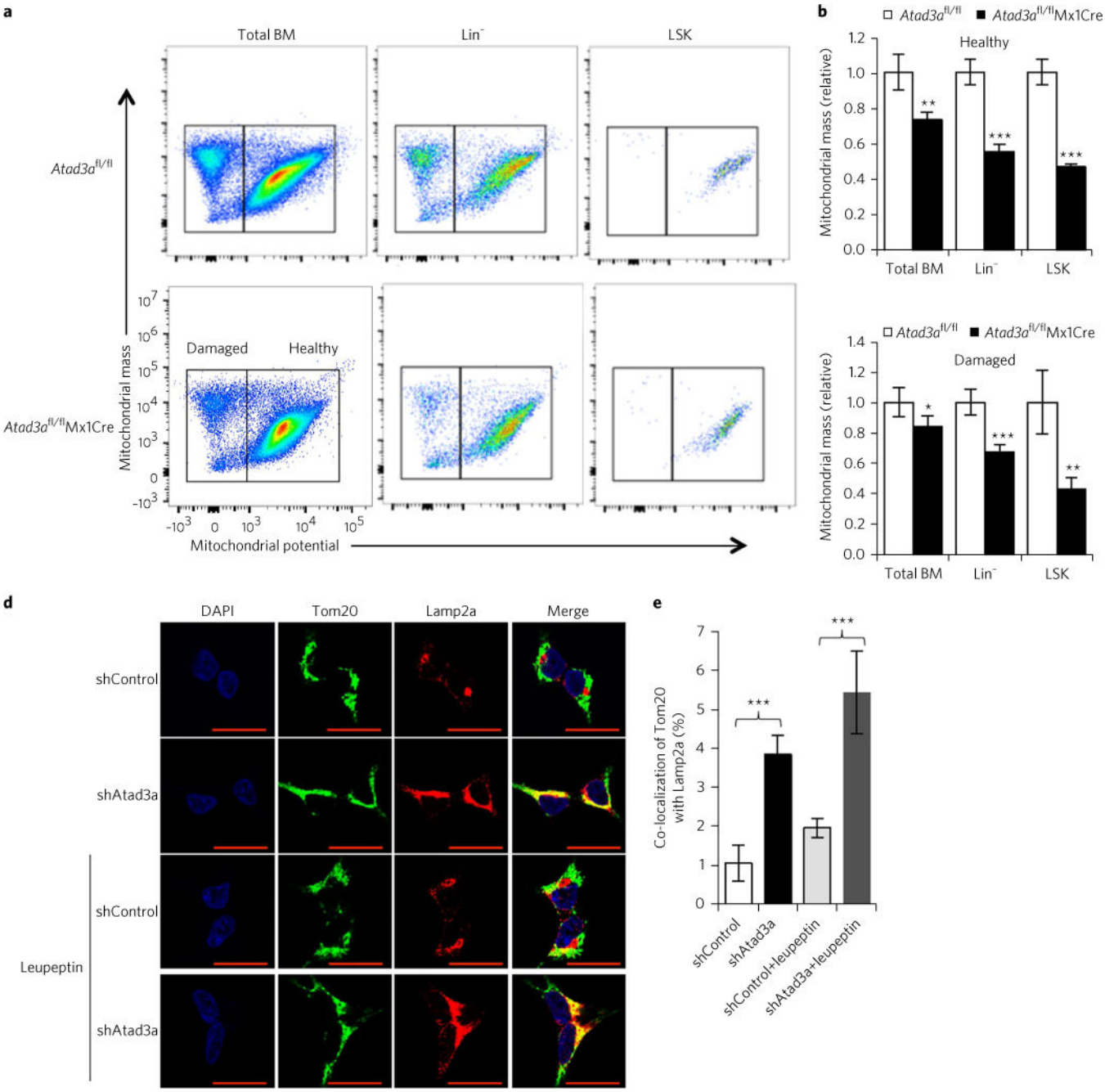

Fig. 5. *Atad3a* deficiency induces mitophagy of both healthy mitochondria and damaged mitochondria

a, Flow cytometry to distinguish populations with high membrane potential (healthy mitochondria) from those with low potential (damaged mitochondria) among hematopoietic cell populations (above plots) from *Atad3a*$^{fl/fl}$ or *Atad3a*$^{fl/fl}$Mx1Cre mice (left margin). **b,c**, Mass of healthy mitochondria (**b**) and damaged mitochondria (**c**) in hematopoietic cell populations (horizontal axis) from *Atad3a*$^{fl/fl}$ or *Atad3a*$^{fl/fl}$Mx1Cre mice (key), presented relative to results obtained for *Atad3a*$^{fl/fl}$ mice. **d**, Confocal microscopy of the co-localization Tom20 and Lamp2a in HEK293T cells expressing (left margin) control (non-

targeting) shRNA (shControl) or *Atad3a*-specific shRNA (shAtad3a) and treated with leupeptin (bottom two rows) or not (top two rows). Scale bar, 20 μm. **e**, Frequency of co-localized Tom20 and Lamp2a in cells as in **d**. *P<0.05, **P<0.01 and ***P<0.001 (Student's t-test). Data are from one experiment representative of two independent experiments (mean±s.d. of n = 4 mice per group (**b,c**) or $n \geq 10$ images per group (**e**)).

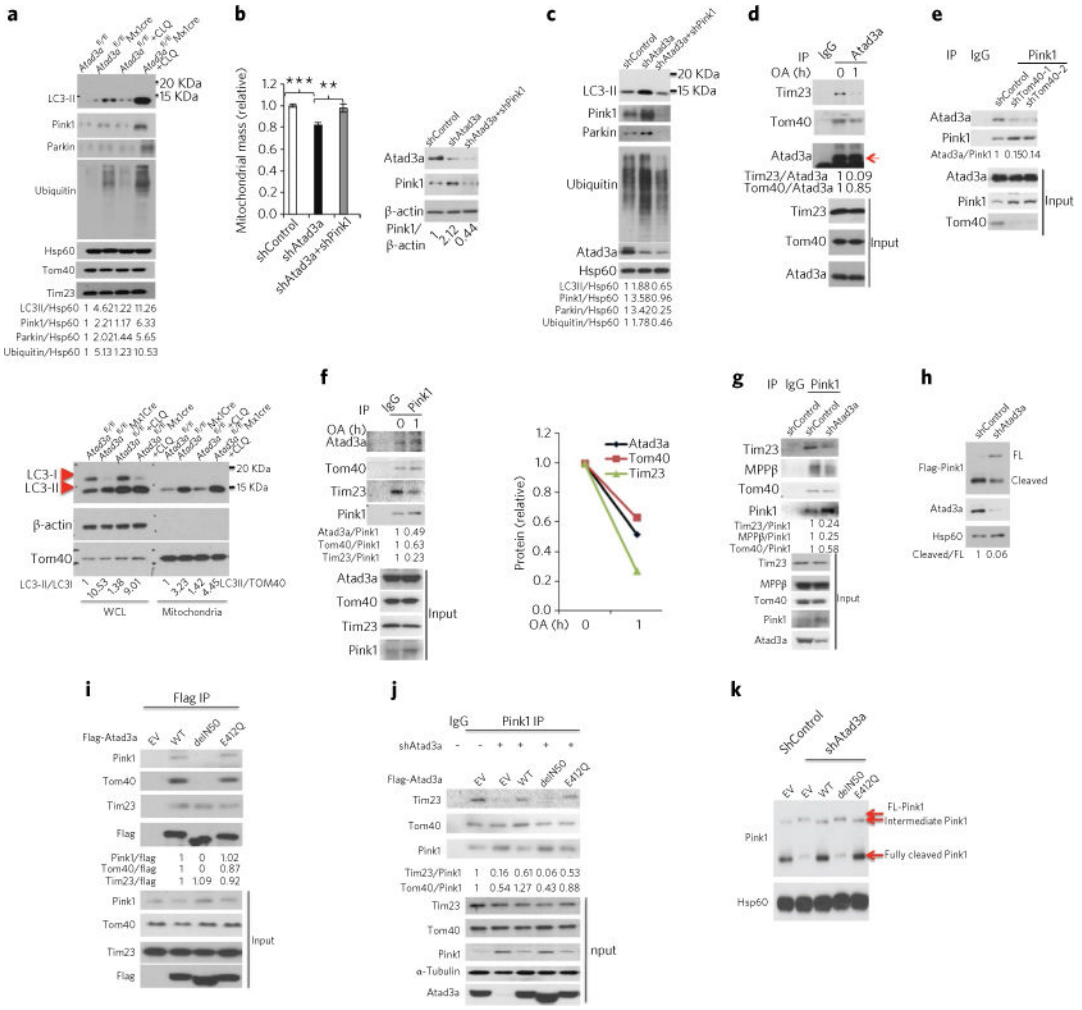

Fig. 6. Atad3a promotes the import of Pink1 into mitochondria to prevent mitophagy

a, Immunoblot analysis of various proteins (left margin) in the mitochondrial fraction of sorted *Atad3a*$^{fl/fl}$ or *Atad3a*$^{fl/fl}$Mx1Cre Lin^{-} cells in the presence (+ CLQ) or absence of chloroquine (top group) and in whole-cell lysates (WCL) (left half) and mitochondrial fractions (right half) of cells as above (bottom); numbers below lanes indicate densitometry analysis of band intensity, relative to that of either the control protein Hsp60 (top group) or LC3I or TOM40 (bottom group). **b**, Mitochondrial mass (left) of HEK293T cells expressing (horizontal axis) control shRNA (shControl) or shRNA specific for *Atad3a* (shAtad3a) or both *Atad3a* and *Pink1* (shAtad3a + shPink1), and immunoblot analysis (right) of Atad3a, Pink1 and β-actin (loading control) (left margin) in cells as at left; mass results (left) are presented relative to those obtained with control shRNA. **c**, Immunoblot analysis of various proteins (left margin) in the mitochondrial fractions of HEK293T cells treated as in **b**; numbers below, as in **a. d**, Immunoblot analysis of Tim23, Tom40 and Atad3a (arrow (right margin)) in HEK293T cells treated for 1 h with 10 μM oligomycin and 4 μM antimycin (OA) or not (0) (above lanes), assessed after immunoprecipitation (IP) with immunoglobulin G (IgG), as a control, or with antibody to Atad3a (above blots); numbers below, densitometry, relative to that of Atad3a; bottom (Input), immunoblot analysis of cells as

above, without immunoprecipitation. **e**, Immunoblot analysis of Atad3a and Pink1 in HEK293T cells expressing (above lanes) control shRNA or either of two shRNAs (−1, −2) specific for *Tomm40* (shTom40), assessed after immunoprecipitation with IgG or antibody to Pink1 (above blots); numbers below, densitometry, relative to that of Pink1; bottom (Input), immunoblot analysis of Atad3a, Pink1 and Tom40 in cells as above, without immunoprecipitation. **f**, Immunoblot analysis (left) of Atad3a, Tom40, Tim23 and Pink1 in HEK293T cells treated for 1 h with OA or not (above lanes), assessed after immunoprecipitation as in **e** (above blots); numbers below, densitometry, relative to that of Pink1; bottom (Input), immunoblot analysis in cells as above, without immunoprecipitation. Right, quantification of immunoprecipitated Atad3a, Tom40, Tim23 (key) in cells as at left, presented as a ratio relative to that of Pink1. **g**, Immunoblot analysis of Tim23, MPPβ, Tom40 and Pink1 in HEK293T cells expressing control or *Atad3a*-specific shRNA (above lanes), assessed after immunoprecipitation as in **e** (above blots); numbers below, densitometry as in e; bottom (Input), immunoblot analysis of cells as above, without immunoprecipitation. **h**, Immunoblot analysis of an *in vitro* mitochondrial importation assay of Flag-tagged Pink1 in mitochondria isolated from cells expressing control or *Atad3a*-specific shRNA (above lanes); numbers below, densitometry analysis of cleaved Pink1, relative to that of full-length (FL) Pink1. i, Immunoblot analysis of endogenous Pink1, Tom40 and Tim23 in cells transfected with empty vector (EV) or to express Flag-tagged wild-type (WT) or mutant Atad3a (above lanes), assessed after immunoprecipitation with antibody to Flag (above blots); numbers below, densitometry relative to that of Flag; bottom (Input), immunoblot analysis of cells as above, without immunoprecipitation. **j**, Immunoblot analysis of Tim23, Tom40 and Pink1 in cells transfected as in i (above lanes) and expressing control (−) or *Atad3a*-specific (+) shRNA (above blots), assessed after immunoprecipitation as in e (above blots); numbers below, densitometry as in **e**; bottom (Input), immunoblot analysis of cells as above, without immunoprecipitation. **k**, Immunoblot analysis of an *in vitro* mitochondrial importation assay of Pink1 in mitochondria isolated from cells treated as in **j**; numbers below, as in **h**. Full-length original scans of blots, Supplementary Fig. 8. $^{**}P<$ 0.0l and $^{***}P<$ 0.00l (one-way ANOVA followed by Bonferroni post-hoc test). Data are from one experiment representative of two independent experiments (**b** (right); mean±s.d. of $n = 3$ biological replicates) or are representative of three (**a,c,d,g**) or two (**b** (left),**e,f,h**) independent experiments.

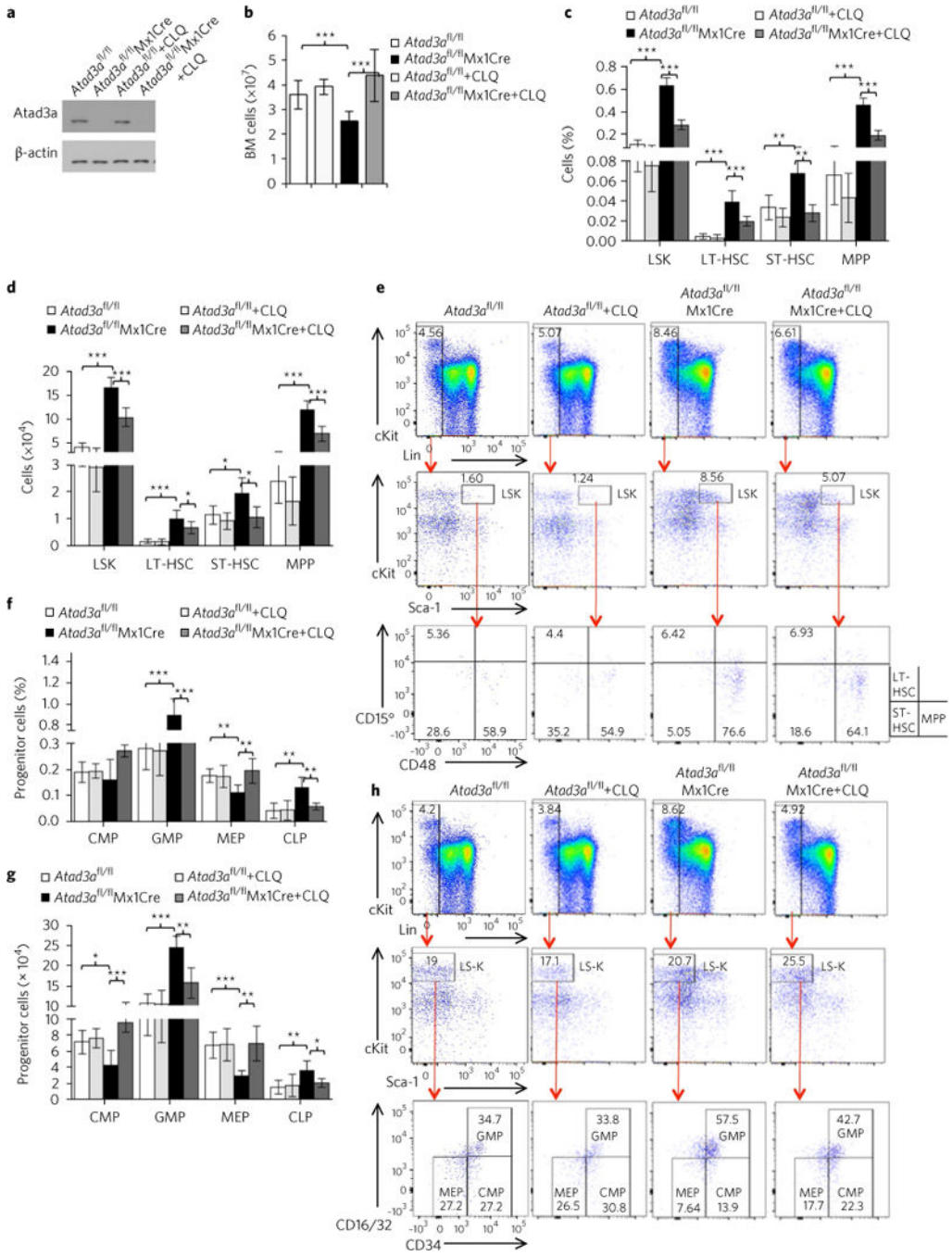

Fig. 7. Hyperactivation of mitophagy causes the aberrant stem cell and progenitor homeostasis in *Atad3a* deficient bone marrow

a, Immunoblot analysis of *Atad3a* in cells from *Atad3a*$^{fl/fl}$ or *Atad3a*$^{fl/fl}$Mx1Cre mice treated with chloroquine or not (above lanes). **b**, Total bone marrow cells in mice as in **a** (key). **c,d**, Frequency (**c**) and number (**d**) of LT-HSCs, ST-HSCs, MPPs and LSK cells (horizontal axis) in the bone marrow of mice as in **a** (key). **e**, Flow cytometry of LT-HSCs, ST-HSCs, MPPs and LSK cells in the bone marrow of mice as in **a** (above plots). **f,g**, Frequency (**f**) and number (**g**) of CMPs, MEPs, GMPs and CLPs (horizontal axis) in the bone marrow of mice

as in **a** (key). **h**, Flow cytometry of CMPs, MEPs and GMPs in the bone marrow of mice as in a (above plots). Numbers in or adjacent to outlined areas (**e,h**) indicate percent cells in each. *P<0.05, **P< 0.01 and ***P< 0.001 (one-way ANOVA followed by Bonferroni post-hoc test (**b–d,f,g**). Data are representative of two independent experiments (**a**) or are from two independent experiments (**b–d,f,g** (average); mean±s.d. of n = 8 mice per group).

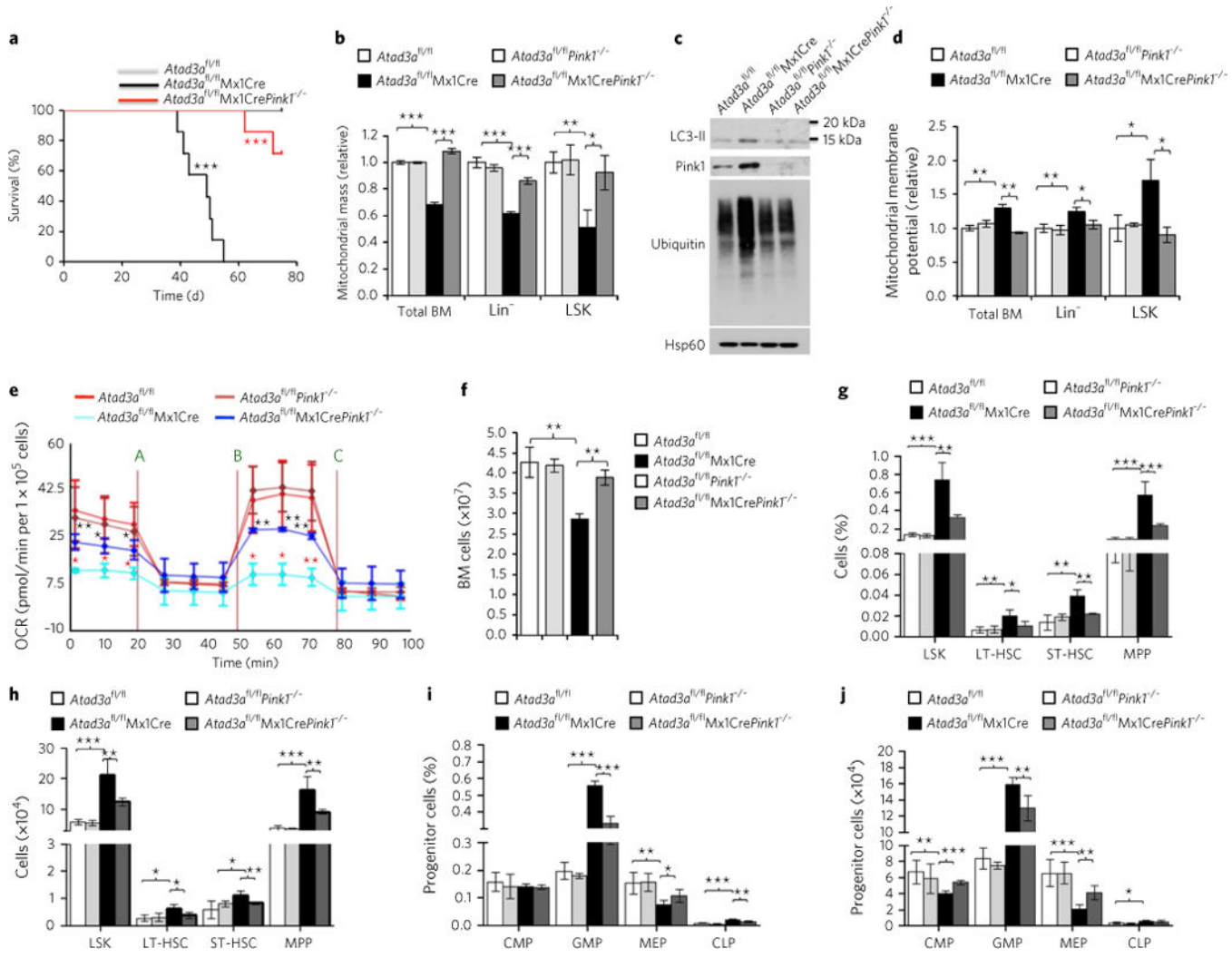

Fig. 8. Pink1-dependent mitophagy causes the aberrant stem-cell and progenitor homeostasis in *Atad3a* deficient bone marrow

a, Survival (Kaplan-Meier analysis) of *Atad3a*$^{fl/fl}$, *Atad3a*$^{fl/fl}$Mx1Cre and *Atad3a*$^{fl/fl}$Mx1CrePink1$^{-/-}$ mice (key) (n = 7 mice per group) at various times (horizontal axis) after injection of poly(I:C). **b**, Mitochondrial mass (as in Fig. 4a) of hematopoietic cell populations (horizontal axis) from *Atad3a*$^{fl/fl}$, *Atad3a*$^{fl/fl}$Mx1Cre, *Atad3a*$^{fl/fl}$*Pink1*$^{-/-}$ and *Atad3a*$^{fl/fl}$Mx1CrePink1$^{-/-}$ mice (key). **c**, Immunoblot analysis of various proteins (left margin) in the mitochondrial fractions of sorted Lin^{-} cells from mice as in **b** (above lanes). Full-length original scans of blots, Supplementary Fig. 8. **d**, Mitochondrial membrane potential (relative to mitochondrial mass, as in Fig. 4b) in hematopoietic cell populations (horizontal axis) from mice as in **b** (key). **e**, Oxygen-consumption rate (as in Fig. 4c) of sorted LSK cells from mice as in **b** (key). **f**, Total bone marrow cells in mice as in **b** (key). **g,h**, Frequency (**g**) and number (**h**) of LT-HSCs, ST-HSCs, MPPs and LSK cells (horizontal axis) in the bone marrow of mice as in **b** (key). **i,j**, Frequency (**i**) and number (**j**) of CMPs, MEPs, GMPs and CLPs (horizontal axis) in the bone marrow of mice as in **b** (key). *P<0.05, **P< 0.01 and ***P<0.001, *Atad3a*$^{fl/fl}$ versus *Atad3a*$^{fl/fl}$Mx1Cre (black asterisks (**a**) or red asterisks (**e**)), *Atad3a*$^{fl/fl}$Mx1Cre versus *Atad3a*$^{fl/fl}$Mx1Cre+Pink1$^{-/-}$ (red asterisks (**a**)) or

(black asterisks (**e**)) (log-rank (Mantel Cox) test (**a**), one-way ANOVA followed by Bonferroni post-hoc test (**b,d–j**)). Data are representative of two independent experiments (**b,d,e**; mean±s.d. of $n = 3$ mice per group), are from one experiment representative of three independent experiments (c) or are from two independent experiments (**f,g–j** (average); mean±s.d. of $n = 5$ mice per group).